SANDIA REPORT

SAND2011-9457
Unlimited Release
Printed January 2012

New Density Functional Theory Approaches for Enabling Prediction of Chemical and Physical Properties of Plutonium and Other Actinides

Ann E. Mattsson

Prepared by
Sandia National Laboratories
Albuquerque, New Mexico 87185 and Livermore, California 94550

Sandia National Laboratories is a multi-program laboratory managed and operated by Sandia Corporation, a wholly owned subsidiary of Lockheed Martin Corporation, for the U.S. Department of Energys National Nuclear Security Administration under Contract DE-AC04-94AL85000.

Approved for public release; further dissemination unlimited.

Sandia National Laboratories

Issued by Sandia National Laboratories, operated for the United States Department of Energy by Sandia Corporation.

NOTICE: This report was prepared as an account of work sponsored by an agency of the United States Government. Neither the United States Government, nor any agency thereof, nor any of their employees, nor any of their contractors, subcontractors, or their employees, make any warranty, express or implied, or assume any legal liability or responsibility for the accuracy, completeness, or usefulness of any information, apparatus, product, or process disclosed, or represent that its use would not infringe privately owned rights. Reference herein to any specific commercial product, process, or service by trade name, trademark, manufacturer, or otherwise, does not necessarily constitute or imply its endorsement, recommendation, or favoring by the United States Government, any agency thereof, or any of their contractors or subcontractors. The views and opinions expressed herein do not necessarily state or reflect those of the United States Government, any agency thereof, or any of their contractors.

Printed in the United States of America. This report has been reproduced directly from the best available copy.

Available to DOE and DOE contractors from
U.S. Department of Energy
Office of Scientific and Technical Information
P.O. Box 62
Oak Ridge, TN 37831

Telephone: (865) 576-8401
Facsimile: (865) 576-5728
E-Mail: reports@adonis.osti.gov
Online ordering: http://www.osti.gov/bridge

Available to the public from
U.S. Department of Commerce
National Technical Information Service
5285 Port Royal Rd
Springfield, VA 22161

Telephone: (800) 553-6847
Facsimile: (703) 605-6900
E-Mail: orders@ntis.fedworld.gov
Online ordering: http://www.ntis.gov/help/ordermethods.asp?loc=7-4-0#online

SAND2011-9457
Unlimited Release
Printed January 2012

New Density Functional Theory Approaches for Enabling Prediction of Chemical and Physical Properties of Plutonium and Other Actinides

Ann E. Mattsson
Computational Shock and Multiphysics MS 1322
Sandia National Laboratories
P.O. Box 5800
Albuquerque, NM 87185-1322
aematts@sandia.gov

Abstract

Density Functional Theory (DFT) based Equation of State (EOS) construction is a prominent part of Sandia's capabilities to support engineering sciences. This capability is based on amending experimental data with information gained from computational investigations, in parts of the phase space where experimental data is hard, dangerous, or expensive to obtain. A prominent materials area where such computational investigations are hard to perform today because of limited accuracy is actinide and lanthanide materials. The Science of Extreme Environment Lab Directed Research and Development project described in this Report has had the aim to cure this accuracy problem.

We have focused on the two major factors which would allow for accurate computational investigations of actinide and lanthanide materials: 1) The fully relativistic treatment needed for materials containing heavy atoms, and 2) the needed improved performance of DFT exchange-correlation functionals.

We have implemented a fully relativistic treatment based on the Dirac Equation into the LANL code RSPt and we have shown that such a treatment is imperative

when calculating properties of materials containing actinides and/or lanthanides. The present standard treatment that only includes some of the relativistic terms is not accurate enough and can even give misleading results. Compared to calculations previously considered state of the art, the Dirac treatment gives a substantial change in equilibrium volume predictions for materials with large spin-orbit coupling. For actinide and lanthanide materials, a Dirac treatment is thus a fundamental requirement in any computational investigation, including those for DFT-based EOS construction.

For a full capability, a DFT functional capable of describing strongly correlated systems such as actinide materials need to be developed. Using the previously successful subsystem functional scheme developed by Mattsson *et.al.*, we have created such a functional. In this functional the Harmonic Oscillator Gas is providing the necessary reference system for the strong correlation and localization occurring in actinides. Preliminary testing shows that the new Hao-Armiento-Mattsson (HAM) functional gives a trend towards improved results for the crystalline copper oxide test system we have chosen. This test system exhibits the same exchange-correlation physics as the actinide systems do, but without the relativistic effects, giving access to a pure testing ground for functionals. During the work important insights have been gained. An example is that currently available functionals, contrary to common belief, make large errors in so called hybridization regions where electrons from different ions interact and form new states.

Together with the new understanding of functional issues, the Dirac implementation into the RSPt code will permit us to gain more fundamental understanding, both quantitatively and qualitatively, of materials of importance for Sandia and the rest of the Nuclear Weapons complex.

Acknowledgment

This work was supported by the Laboratory Directed Research and Development Program at Sandia National Laboratories. We also acknowledge some support from the Nuclear Energy Advanced Modeling and Simulation (NEAMS) programs Fundamental Methods and Models element. Sandia National Laboratories is a multi-program laboratory managed and operated by Sandia Corporation, a wholly owned subsidiary of Lockheed Martin Corporation, for the U.S. Department of Energy's National Nuclear Security Administration under contract DE-AC04-94AL85000.

Contents

Nomenclature **11**

1 Introduction and Motivation **13**

2 Density Functional Theory **17**

3 The Dirac Kohn-Sham Equations **19**

The Dirac Kohn-Sham Equations 19

Neglecting the Orbital Current: From current functionals to density functionals 20

The radial equation: Dirac, scalar relativistic, variational spin-orbit, and non-relativistic treatments 21

Summary of work 22

4 An Exchange-Correlation Functional for actinides **23**

The sub-system functional scheme 23

The Harmonic Oscillator Model system: Confinement physics 25

The Electron Localization Function: Identifying confinement physics in real systems 25

A functional for confined systems 28

5 Summary and Conclusion **31**

References **32**

Appendix

A Implementational details for DiracRSPt: The transition to full Dirac bases in the framework of RSPt **37**

A.1 Introduction: the transition from RSPt to Dirac 37

A.2 Matrix Elements 41

B Details of an exchange-correlation functional for confined systems **47**

B.1 Kinetic Energy density of HO gas 47

B.2 parameterization of the exchange energy per particle for HO gas 48

List of Figures

1.1 The foundation of Science Based Engineering is to build bridges from the fundamental Laws of Nature up to the Engineering codes, bridging several length and time scales. In this figure two different paths are depicted. The upper one is quite complicated and illustrates the general problem of bridging several different scales. The lower path is already in use at Sandia. For Equation of State construction, data provided by Density Functional Theory (DFT) based calculations are used in addition to experimental data. The DFT calculations are used in two ways, either directly or as a provider of forces in a Molecular Dynamics scheme. 15

2.1 The exact functional would give the exact density, ρ, and thus the exact properties via density functionals, $F[\rho]$. The unknown wave function density functional, $\Psi[\rho]$, would in this case give all properties that can be calculated from the Schrödinger equation exactly. However, the mean field view of using the KS orbitals as approximate electron wave functions would be approximate. Only the density and properties calculated via density functionals are guaranteed to be exact. The quality of a functional can thus not be judged by how well it reproduces wave function derived properties. From Reference 18. 18

4.1 A new general functional combining three subsystem functionals using an interpolation index. Each subsystem functional is based on a different model system, the uniform electron gas, the Airy gas, and the Mathieu gas, describing three different physics situations. The additional subsystem functional compared to AM05, based on the Mathieu gas, describes the exchange- correlation contribution from a situation where the density is confined in space. 24

4.2 The ELF and the dimensionless exchange energy per particle $l\epsilon_x$ for two HO systems, one strongly confined and one less confined, as a function of the dimensionless spatial coordinate $\bar{z}$, with $\bar{z} = 0$ in the center of the harmonic well. The green dash-dotted lines in the upper panels show the ELF. In the lower panels the exact $l\epsilon_x$ is shown in solid black, the approximations by LDA and AM05 are represented by dashed red and dotted blue lines, respectively. 26

4.3 The contours are surrounding spacial regions where the ELF value is larger than 0.83 (dark blue) and 0.77 (light blue). 4 Cu atoms (dark, brown) connect the one O atom (light, gray) in the center. 27

4.4 Test of the post-correction scheme we use for preliminary testing of the HAM functional, shown in Figure 4.5. 29

4.5 Post-correction results with the new HAM functional. Compared to LDA, AM05, and PBE the HAM functional correctly gives a smaller equilibrium volume for CuO. 30

Nomenclature

Dirac The Dirac Equation: The relativistic quantum mechanical wave equation describing electrons in relativistic matter, such as in heavy materials like actinides.

SE The Schrödinger Equation: The non-relativistic limit of the Dirac Equation, sufficiently accurate to describe electrons in lighter materials.

DFT Density Functional Theory: The formally exact reformulation of the wave-function based Shrödinger and Dirac Equations in terms of density and currents.

KS The Kohn-Sham Equations: A calculational approach derived from the Dirac/SE using DFT. These are the equations implemented in DFT codes.

Functional A short name for an approximation for the Exchange-Correlation functional which is the only part of DFT that needs to be approximated. The functional sets the possible accuracy of DFT calculations.

NR Non relativistic treatment: A treatment based on the SE.

SR Scalar Relativistic treatement: An approximation derived from the Dirac Equation, taking some of the relativistic effects into account.

SO Spin-orbit coupling: Another relativistic term that can be included in DFT calculations. It can be included on top of SR or NR based treatments.

LMTO Linear Muffin Tin Orbital: A calculational method used in the RSPt code and in the new Dirac code.

LAPW Linear Augmented Plane Wave: Another calculational method. It is considered the implemetational method that gives the most accurat DFT results. Other methods are usually verified against this method.

plane-wave code A code using plane waves as a basis set. This is the computationally most effective approach because Fourier Transforms can be used. Calculations can also be systematically improved by increasing the number of basis functions used, usually specified by the so called 'cut-off'. However, describing core electrons accurately requires a very large cut-off, leading to expensive calculations. The plane-wave approach thus is mostly used together with pseudo-potentials (see below).

all-electron code A code treating all electrons explicitly. LMTO and LAPW codes are all-electron.

pseudo-potential code The chemically inert core electrons are treated in a collective way via pseudo potentials, which increase the computational efficiency considerably. A number of different approaches exist, they all are verified by comparing to all-electron, usually LAPW, results.

PAW Projected Augmented Wave: The pseudo potential technique today considered the most accurate.

RSPt Relativistic Spin-Polarised test: The name of the LMTO code we have modified to include a Dirac treatment.

VASP Vienna *Ab-initio* Simulation Package: A plane wave, pseudo potential (PAW), DFT code extensively used at Sandia.

core electron An electron close to the nuclei. In an LMTO or LAPW treatment these electrons are considered inert and their properties only depends on the closest nuclei. In a pseudo-potential code the effect of the core electrons on the valence electrons are included via pseudo potentials.

semi-core electron An electron that is intermediate between a core and a valence electron. It has the same angular momentum quantum number as some of the valence electrons but has a lower principal quantum number (it is in a lower shell). For the heavier nuclei these electrons need to be treated as valence electrons.

valence electron The outermost electrons are valence electrons and their properties are dependent on many nuclei. These electrons are forming bonds that hold a solid or molecule together.

Chapter 1

Introduction and Motivation

Density functional theory (DFT) is the preferred computational method for exploring materials properties and Sandia scientists are at the forefront of DFT-based equation of state (EOS) construction, where information from both experiments and computational investigations are used (See Figure 1.1). However, present DFT techniques are not adequate for f-electron materials, hampering our ability to computationally investigate many materials of high interest to DOE/NNSA, such as plutonium (Pu), under conditions where experiments are hard and/or very expensive to perform.

DFT[12,16] is a formally exact reformulation of the Schrödinger Equation (SE) for the ground state of an electron system. Since the DFT equations are far easier to solve than the SE, DFT has become the preferred computational method for exploring properties of materials. One recent example of a Sandia effort in this area is the resent use of DFT results combined with Z experiments to construct a new Quartz standard leading to the resolution of a most important discrepancy between flyer plate and laser driven shock data for deuterium.[14] Another example is the same type of work for Xenon,[26] a material of importance for DOE. Here DFT results helped both in showing that the available Equation of State (EOS) tables were insufficiently accurate at high pressures and in the construction of a new, more accurate, EOS.

Despite the success of DFT in most of materials science, there are still areas where the performance of DFT has been less satisfactory. The chemical and physical properties of actinides form such an area. There are three main reasons for this:

1. The density functional that defines the mapping between the SE and DFT is not known exactly, and the approximation used for the functional completely governs the accuracy of DFT calculations. The functionals created to date all perform equally badly for actinide properties. For example, the equilibrium volume of Pu is underestimated by 10-20% with the best performing functional (see e.g. Refs. 29 and 13).

2. It is critical to include electron spin and relativistic effects when calculating properties of the actinides (see e.g. Refs. 13 and23). A full relativistic treatment is required to obtain the needed precision for actinide properties. However, most all-electron, full-potential codes only use a perturbative treatment of the spin-orbit interaction, which gives even smaller equilibrium volume for, e.g. Pu.[7]

3. Since actinides and lanthanides contain f-electrons that are interacting with both core and valence electrons, it is crucial to use a full potential, all-electron code for the calculations. All-electron codes are much slower than the pseudo-potential codes usually used for complex materials science investigations. Going beyond the basic properties of actinides and lanthanides thus requires a speed up of the calculations by using state-of-the-art algorithms and advanced computer science methods.

We have so far only been addressing the two fundamentally accuracy-limiting deficiencies mentioned above, the failure of existing density functionals and the perturbative relativistic treatment. However, our focus on developing a simple functional via the subsystem functional scheme has the potential to give a functional that is not only accurate but also leads to calculations that are one to three orders of magnitude faster to perform than using functionals developed with other techniques.

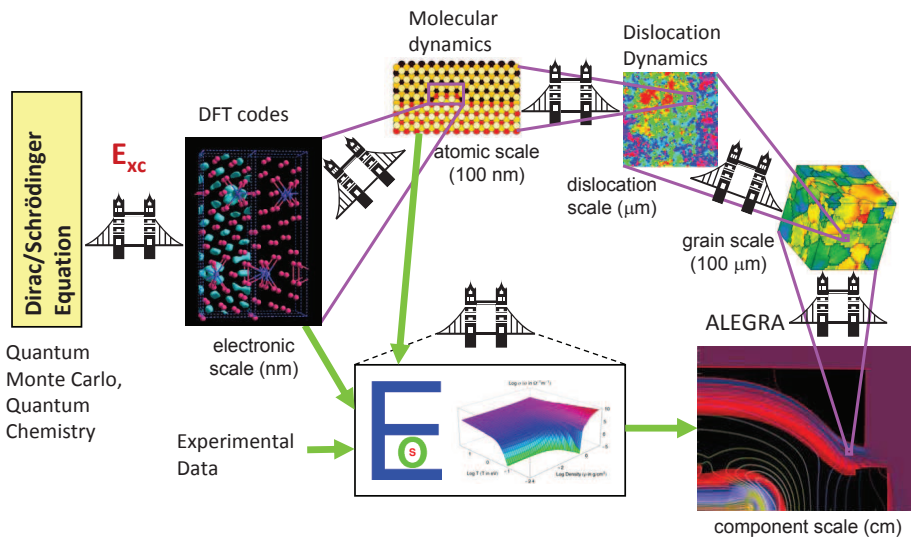

Figure 1.1. The foundation of Science Based Engineering is to build bridges from the fundamental Laws of Nature up to the Engineering codes, bridging several length and time scales. In this figure two different paths are depicted. The upper one is quite complicated and illustrates the general problem of bridging several different scales. The lower path is already in use at Sandia. For Equation of State construction, data provided by Density Functional Theory (DFT) based calculations are used in addition to experimental data. The DFT calculations are used in two ways, either directly or as a provider of forces in a Molecular Dynamics scheme.

Chapter 2

Density Functional Theory

Density Functional Theory (DFT) is an exact reformulation of the fundamental law of nature governing the behavior of electrons. If electrons are in materials with heavy ions, the fundamental law to use is the Dirac equation. For materials composed of lighter ions, the non-relativistic limit of the Dirac equation, the Schrödinger equation, might be used. We will discuss different levels of approximations to the Dirac equation in the next chapter.

Density Functional Theory was first developed based on the Schrödinger equation. Using the Hohenberg-Kohn theorem,[12] the Shrödinger equation, which decide the electronic properties of a material via many-body electronic wave-functions, can be cast in the form of the Kohn-Sham (KS) equations, which instead decide the behavior of ground state electrons via auxiliary non-interacting single particle Kohn-Sham orbitals forming the true electron density of the material. The key point is that solving for non-interacting single particles is a much less demanding task than solving for many-body wave-functions.

Despite the theory in itself being exact, approximations for the *Exchange-Correlation functional* still need to be done since the form of this object is unknown. The accuracy of the approximation for the Exchange-Correlation functional is the factor that decides the ultimately attainable accuracy of the calculations. No calculations based on DFT can ever give better results than what this approximation allows. If the 'divine'[19] functional was known, however, the KS equations would yield the exact same results as the fundamental law of nature, the Schrödinger Equation.

The KS equations are often interpreted as the equations of electrons moving in a field formed by all the other electrons, so called mean-field theory. From a mean-field theory perspective the KS orbitals can be interpreted as approximations for the true many-body electron wave-functions. This alternative interpretation of the KS equations can be very fruitful if handled correctly, but it also has created, and is creating, a lot of confusion in the field. In Figure 2.1 we try to compare the two views.

Density Functional Theory has later been extended to be based on the Dirac equation, which we will discuss next.

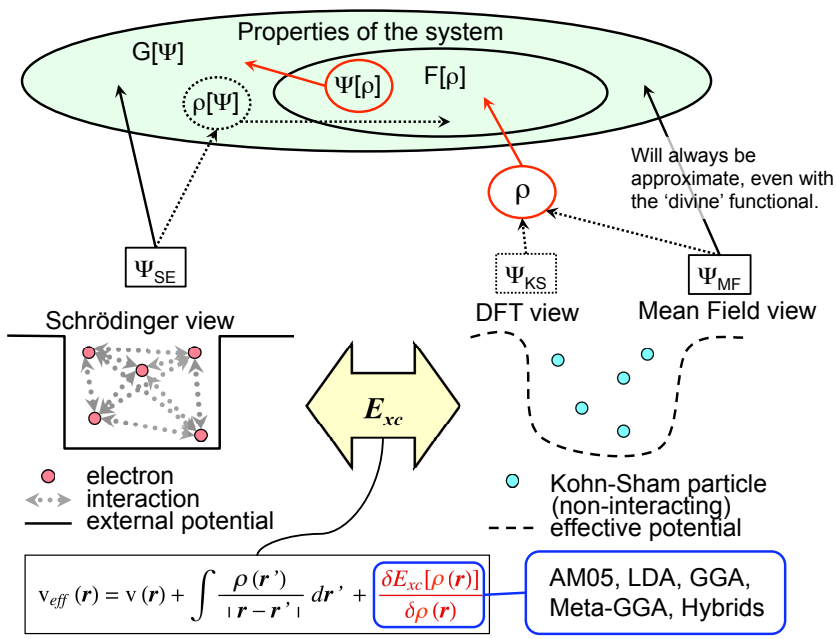

Figure 2.1. The exact functional would give the exact density, ρ, and thus the exact properties via density functionals, $F[\rho]$. The unknown wave function density functional, $\Psi[\rho]$, would in this case give all properties that can be calculated from the Schrödinger equation exactly. However, the mean field view of using the KS orbitals as approximate electron wave functions would be approximate. Only the density and properties calculated via density functionals are guaranteed to be exact. The quality of a functional can thus not be judged by how well it reproduces wave function derived properties. From Reference 18.

Chapter 3

The Dirac Kohn-Sham Equations

To properly account for relativistic effects in materials containing heavy ions, the Dirac Kohn-Sham equations should be used, not the ordinary Schrödinger Equation based Kohn-Sham equations. We discuss the various approximations to the full Dirac KS scheme that are usually done, and their possible consequences. We also discuss the prospects of eliminating a few of the approximations.

The Dirac Kohn-Sham Equations

The relativistic Kohn-Sham equations are discussed in Dreizler and Gross's book (Ref. 6). Transferring their Eqns. (8.16)-(8.17b) to the notation we will use in this report we get:

$$\left(c\,\boldsymbol{\alpha}\cdot\left(\boldsymbol{p}-\frac{e\boldsymbol{A}_{\mathit{eff}}}{c}\right)+\begin{pmatrix} I & 0 \\ 0 & I \end{pmatrix} V_{\mathit{eff}}(\boldsymbol{r})+\beta\, mc^2\right)\psi_n(\boldsymbol{r}) = E_n\,\psi_n(\boldsymbol{r}) \tag{3.1}$$

with

$$V_{\mathit{eff}}(\boldsymbol{r}) \;=\; -e\left(A^0_{\mathit{ext}}(\boldsymbol{r})+\int d^3r'\frac{J^0(\boldsymbol{r'})}{|\boldsymbol{r}-\boldsymbol{r'}|}+\frac{\delta E_{xc}[J^\mu]}{\delta J^0(\boldsymbol{r})}\right) \tag{3.2}$$

and

$$e\boldsymbol{A}_{\mathit{eff}}(\boldsymbol{r}) \;=\; -e\left(\boldsymbol{A}_{\mathit{ext}}(\boldsymbol{r})+\int d^3r'\frac{\boldsymbol{J}(\boldsymbol{r'})}{|\boldsymbol{r}-\boldsymbol{r'}|}+\frac{\delta E_{xc}[J^\mu]}{\delta \boldsymbol{J}(\boldsymbol{r})}\right) \tag{3.3}$$

for all negative and positive energy orbitals. The matrices are defined as

$$\alpha_k \;=\; \begin{pmatrix} 0 & \sigma_k \\ \sigma_k & 0 \end{pmatrix} \qquad \beta=\begin{pmatrix} I & 0 \\ 0 & -I \end{pmatrix} \qquad I=\begin{pmatrix} 1 & 0 \\ 0 & 1 \end{pmatrix} \tag{3.4}$$

and σ_k denotes the Pauli matrices. The Dirac 4-component spinors, ψ_n, can be represented as single-row matrices:

$$\psi_n = \begin{pmatrix} \psi_{1,n} \\ \psi_{2,n} \\ \psi_{3,n} \\ \psi_{4,n} \end{pmatrix} = \begin{pmatrix} \psi_{A,n} \\ \psi_{B,n} \end{pmatrix} . \tag{3.5}$$

The conserved current, $J^\mu = (J^0, \boldsymbol{J})$, is analogous to the density in non-relativistic DFT, and is thus the conserved current of the real system that can be calculated from the above spinor solutions to the relativistic KS equations:

$$J^\mu = (J^0, \boldsymbol{J}) = -e \sum_n \left(\psi_n^\dagger \psi_n, \psi_n^\dagger \boldsymbol{\alpha}\, \psi_n \right) , \tag{3.6}$$

Note that the energy includes the rest mass energy, and that the available energy for bonding and kinetic energy is $E_n - mc^2$.

It is well known that the vacuum expectation value of the current operator is non-zero; pairs of electron-positrons can spontateously be created in vacuum, so called vacuum polarization. If this vacuum polarization is neglected the current becomes:[6]

$$J^\mu = -e \sum_{-mc^2 < E_n < E_F} \left(\psi_n^\dagger \psi_n, \psi_n^\dagger \boldsymbol{\alpha}\, \psi_n \right) . \tag{3.7}$$

Neglecting the Orbital Current: From current functionals to density functionals

However, in non-relativistic DFT, the currents $\boldsymbol{J} = -e \sum \psi_n^\dagger \boldsymbol{\alpha} \psi_n$, that couple to the effective vector potential $\boldsymbol{A}_{\mathit{eff}}$ in the Hamiltonian in Eqn. (3.1), are not used, and in order to connect to, and be able to use functionals created for, NR DFT, we would rather use the spin-density

$$\boldsymbol{S} = - \sum_{-mc^2 < E_n < E_F} \psi_n^\dagger \, \beta \, \boldsymbol{\Sigma} \, \psi_n \, . \tag{3.8}$$

Here

$$\Sigma_k = \begin{pmatrix} \sigma_k & 0 \\ 0 & \sigma_k \end{pmatrix} \tag{3.9}$$

It can be shown that, for time-independent problems, $\boldsymbol{J}$ can be written as (Gordon decomposition, see for example Sakurai, Ref. 27):

$$\boldsymbol{J} = \boldsymbol{I} + \mu_B \, \nabla \times \boldsymbol{S} \tag{3.10}$$

where

$$\boldsymbol{I} = \frac{e}{2mc} \sum_{-mc^2<E_n<E_F} \left\{ \psi_n^\dagger \, \beta \left[\left(\boldsymbol{p} - \frac{e\boldsymbol{A}_{\mathit{eff}}}{c} \right) \psi_n \right] + \left[\left(\boldsymbol{p} - \frac{e\boldsymbol{A}_{\mathit{eff}}}{c} \right) \psi_n \right]^\dagger \beta \, \psi_n \right\} . \tag{3.11}$$

By neglecting the orbital current, $\boldsymbol{I}$, and only using the spin-density current, the $e\,\boldsymbol{\alpha} \cdot \boldsymbol{A}_{\mathit{eff}}$ in the Hamiltonian in Eqn. 3.1 can be 'simplified', and the Hamiltonian becomes

$$\left(c\,\boldsymbol{\alpha} \cdot \boldsymbol{p} + \mu_B \, \beta \, \boldsymbol{\Sigma} \cdot \boldsymbol{B}_{\mathit{eff}} + \begin{pmatrix} I & 0 \\ 0 & I \end{pmatrix} V_{\mathit{eff}}(\boldsymbol{r}) + \beta \, mc^2 \right) \psi_n(\boldsymbol{r}) = E_n \, \psi_n(\boldsymbol{r}) \tag{3.12}$$

where $\boldsymbol{B} = \nabla \times \boldsymbol{A}$ and μ_B is the Bohr magneton. Eqn. (3.3) should be replaced by

$$\mu_B \boldsymbol{B}_{\mathit{eff}}(\boldsymbol{r}) \;=\; \left(\mu_B \boldsymbol{B}_{\mathit{ext}}(\boldsymbol{r}) + \int d^3r' \frac{\boldsymbol{M}(\boldsymbol{r'})}{|\boldsymbol{r} - \boldsymbol{r'}|} + \frac{\delta E_{xc}[J^0, \boldsymbol{M}]}{\delta \boldsymbol{M}(\boldsymbol{r})} \right) , \tag{3.13}$$

where $\boldsymbol{M} = \mu_B \boldsymbol{S}$.

For more details see the supplemental material to Ref. 5.

The radial equation: Dirac, scalar relativistic, variational spin-orbit, and non-relativistic treatments

The difference in the relativistic treatments is readily described in the radial equations. Assuming a spherically symmetric potential $V_{\mathit{eff}}(\boldsymbol{r}) = V(r)$ and $\boldsymbol{B}_{\mathit{eff}} = 0$, Equation 3.12 reduces to

$$c\,\boldsymbol{\sigma} \cdot \boldsymbol{p} \, \psi_{B,n}(\boldsymbol{r}) \;=\; (E_n - V(r) - mc^2) \, \psi_{A,n}(\boldsymbol{r}) \tag{3.14}$$

$$c\,\boldsymbol{\sigma} \cdot \boldsymbol{p} \, \psi_{A,n}(\boldsymbol{r}) \;=\; (E_n - V(r) + mc^2) \, \psi_{B,n}(\boldsymbol{r}) \; . \tag{3.15}$$

By separation of angular and radial variables in Eqns. 3.14 and 3.15 (for details see for example Sakurai[27]) we arrive at the Dirac radial equations

$$-c\frac{d\,f_\kappa}{dr} - \frac{(1-\kappa)c}{r} \, f_\kappa \;=\; (E_n - V(r) - mc^2) \, g_\kappa \tag{3.16}$$

$$c\frac{d\,g_\kappa}{dr} + \frac{(1+\kappa)c}{r} \, g_\kappa \;=\; (E_n - V(r) + mc^2) \, f_\kappa \, . \tag{3.17}$$

Setting $e = E_n - mc^2$ and $M = m + (e - V(r))/2c^2$ and eliminating f_κ results in the upper component radial equation

$$-\frac{1}{2M}\left(g_\kappa^{''}+\frac{2}{r}\,g_\kappa^{'}-\frac{\ell(\ell+1)}{r^2}\,g_\kappa\right)-\left(g_\kappa^{'}+\frac{(1+\kappa)}{r}\,g_\kappa\right)\frac{d}{dr}\frac{1}{2M}+V(r)\,g_\kappa=e\,g_\kappa\,, \quad (3.18)$$

where we have also used that $\kappa(\kappa+1)=\ell(\ell+1)$ for both signs of κ.

In the fully relativistic Dirac radial equation in 3.18 the spin and orbital momenta are not independent constants of motion but coupled, a coupling represented by κ, the eigenvalue of the operator $\hat{K}=(\boldsymbol{\sigma}\cdot\boldsymbol{\mathcal{L}}+1)\,\beta$, where $\boldsymbol{\mathcal{L}}$ is the ordinary orbital momentum operator that squared gives eigenvalue $\ell(\ell+1)$.

If the κ-dependent term is dropped, as suggested by Harmon and Koelling,[15] the spin and orbital momenta are decoupled and only ℓ is needed for the description of the resulting solution:

$$-\frac{1}{2M}\left(g_\ell^{''}+\frac{2}{r}\,g_\ell^{'}-\frac{\ell(\ell+1)}{r^2}\,g_\ell\right)-g_\ell^{'}\frac{d}{dr}\frac{1}{2M}+V(r)\,g_\ell=e\,g_\ell\,. \quad (3.19)$$

This is the scalar relativistic (SR) treatment. The term neglected in the SR treatment (as compared to the Dirac treatment) is the spin-orbit (SO) coupling.

In the RSPt code,[1] as in other LMTO and LAPW codes, the SR treatment is used to form the basis but the SO term can be included in the calculation variationally. However, the SR basis is limited in its possibility to describe the SO term[23] and this is the motivation to this project's focus on using the Dirac treatment for the basis instead. The differences between a Dirac, a SR + SO, and a SR treatment for Th is dicussed in an article to be published.[31]

In the non-relativistic limit, $M\rightarrow m$ and from Equation 3.18 (or 3.19) we obtain

$$-\frac{1}{2M}\left(g_\ell^{''}+\frac{2}{r}\,g_\ell^{'}-\frac{\ell(\ell+1)}{r^2}\,g_\ell\right)+V(r)\,g_\ell=e\,g_\ell\,, \quad (3.20)$$

the radial Schrödinger Equation (SE).

Summary of work

The Dirac treatment represented by Equations 3.12, 3.13, and 3.2, has been implemented into a new code, diracRSPt, based on the RSPt code[1] (for details on the implementation, see Appendix A). DiracRSPt has been kept tied as closely as possible to the original RSPt code as to allow for accurate comparison between Dirac, SR+SO, and SR treatments. Such a comparison has been done for Thorium (Th), Gold (Au), and Aluminum (Al), described in Reference 31, with the important and far-reaching result that a Dirac treatment is imperative for Th and other actinide and rare-earths.

Chapter 4

An Exchange-Correlation Functional for actinides

We have been focusing on the subsystem functional (SSF) approach to new, better, exchange-correlation functionals (see References 2, 17, and 20). The SSF scheme differs from the two conventional approaches to functional construction. The first of these uses exact constraints derived for the exact (but unknown) functional and has resulted in for example the PBE[24] functional. The other approach is prevailing in the chemistry community and is based on fitting to experimental data. These have been the approaches for many years and have resulted in a plentitude of different functionals. This not only shows the important role that DFT calculations play in science, but also that no single functional is working for all systems. And, as stated above, none of them are working for actinides. Something new is required.

The sub-system functional scheme

The SSF scheme is a new and promising approach. We have explored what this scheme can do for f-electron systems. We recently assessed the performance of several functionals for solid state systems.[21] This study shows that the AM05 functional,[3] the very first functional constructed by the SSF scheme, has the same performance as the most accurate functionals constructed to date, but with a computational speed faster by one to three order of magnitudes. AM05 can replace all other functionals for these systems; the previously needed choice between LDA and PBE/PW91 is no longer needed. Subsystem functionals are designed to model the exchange-correlation energy of model systems that represent specific types of physics. LDA is a subsystem functional in that it is modeled from the exact results for the uniform electron gas. An improved global functional can be obtained by merging different subsystem functionals. AM05 is built from two model-systems: the uniform electron gas and the jellium surface/Airy Gas system. However, other types of physics also need to be included in a functional for f-electrons. In Figure 4.1 this approach is depicted in a schematic way. The SSF approach is thoroughly described in Reference 20.

While f-electrons has been our focus in this project it is important to remember that

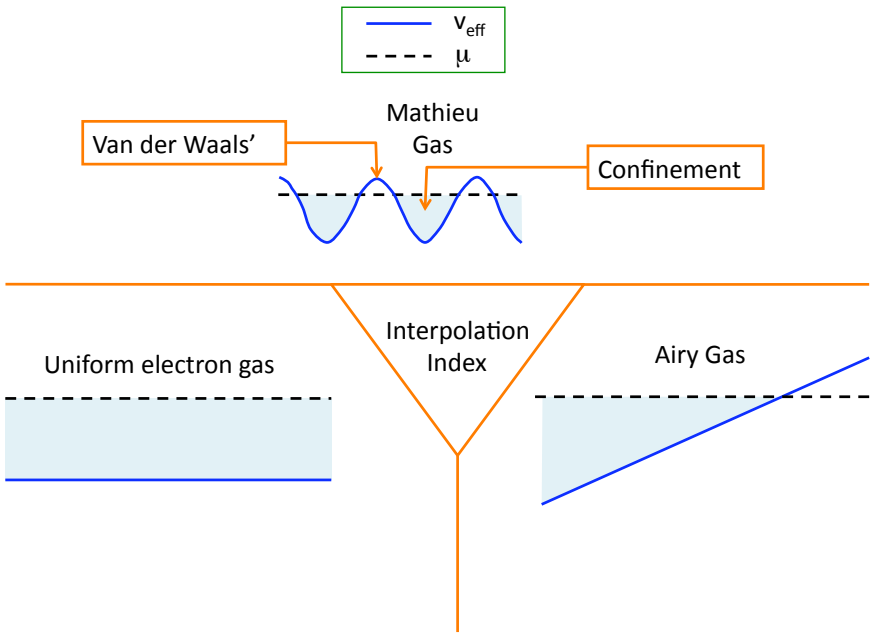

Figure 4.1. A new general functional combining three subsystem functionals using an interpolation index. Each subsystem functional is based on a different model system, the uniform electron gas, the Airy gas, and the Mathieu gas, describing three different physics situations. The additional subsystem functional compared to AM05, based on the Mathieu gas, describes the exchange- correlation contribution from a situation where the density is confined in space.

a new functional that is accurate for f-electron systems still needs to have a similar accuracy for all other materials of interest, like oxygen and water, in order to be truly useful.

The Harmonic Oscillator Model system: Confinement physics

In Reference 10 we describe our work on understanding how DFT functionals work in confined systems. We use the Harmonic Oscillator (HO) model system for this investigation. The HO system is the limiting case for the Mathieu gas (MG) depicted in Figure 4.1, when the amplitude of the sinusoidal wave is large, or equivalently, the chemical potential is small. For details on the HO model system see Reference 10. We show that commonly used functionals makes large errors in the higher density region in the center of the harmonic well, an error that is proportional to the degree of confinement. In Figure 4.2 the lower panels show this error, and it is clearly seen that the error is substantial in the strongly confined system.

The Electron Localization Function: Identifying confinement physics in real systems

In Reference11 we describe our work on identifying and correcting for the confinement physics in a real system, a transition metal oxide, CuO. We have chosen the CuO system because it has the same kind of confinement physics included as actinides, but with no relativistic effects. This allows us to investigate the, for actinides, important confinement physics without the issues related to the Dirac Equation discussed in Chapter 3. The CuO system is also interesting in itself. From a functional perspective since LDA, AM05, and PBE, all three, give too LARGE equilibrium volumes, contrary to the usual trend of LDA too small, AM05 good, and PBE too large.[9,21] From a physics viewpoint CuO is interesting since it does not crystallize in the, for transition metal oxides, usual rocksalt structure, and many signatures of physics of interest in the cuprate high temperature superconductors are also present in this system.

A first observation, shown in Figure 4.2, is that the error common functionals make in the HO system is correlated to the largeness of the so called Electron Localization Function (ELF). The ELF is describing the degree of localization of an electron. Electrons are fermionic particles which means they cannot occupy the same quantum state. The other type of fundamental particle, the boson, has no such restrictions, and bosons can thus 'condensate' into the same state, so called Bose-Einstein condensate. In a uniform electron gas, all electrons have the same potential energy, and they need to differentiate with the help of their kinetic energy. By construction the ELF

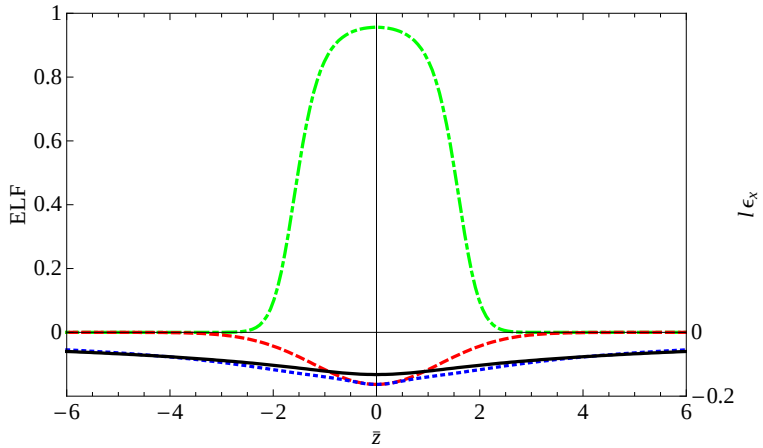

(a) A strongly confined system ($\alpha = 0.06$).

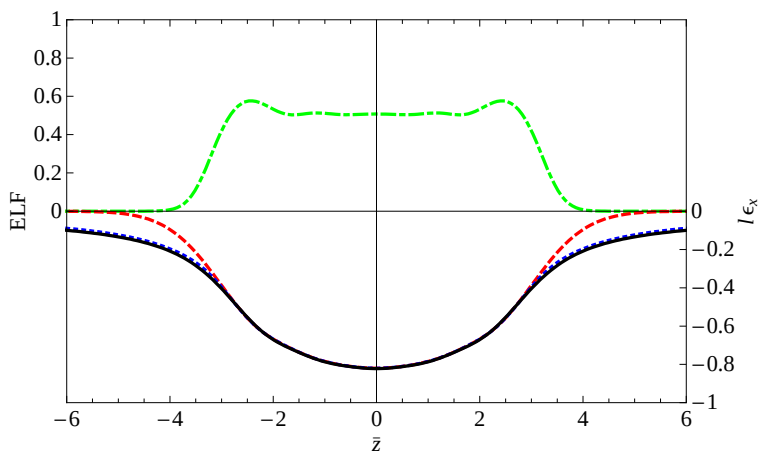

(b) A less confined system ($\alpha = 5.40$).

Figure 4.2. The ELF and the dimensionless exchange energy per particle $l\epsilon_x$ for two HO systems, one strongly confined and one less confined, as a function of the dimensionless spatial coordinate $\bar{z}$, with $\bar{z} = 0$ in the center of the harmonic well. The green dash-dotted lines in the upper panels show the ELF. In the lower panels the exact $l\epsilon_x$ is shown in solid black, the approximations by LDA and AM05 are represented by dashed red and dotted blue lines, respectively.

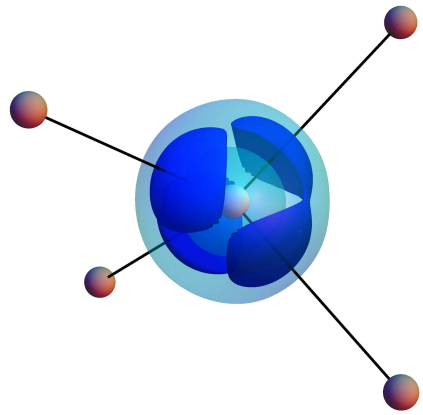

Figure 4.3. The contours are surrounding spacial regions where the ELF value is larger than 0.83 (dark blue) and 0.77 (light blue). 4 Cu atoms (dark, brown) connect the one O atom (light, gray) in the center.

has a value of 1/2 for such electrons. In Figure 4.2(b) it is seen that for the less confined system the electrons in the center of the well become uniform electron gas like, and LDA is a valid approximation for their exchange energy. A value close to 1, as in Figure 4.2(a), instead indicates that electron has its own set of pure quantum numbers and does not need to differentiate itself with the help of different kinetic energies but can have a bosonic like kinetic energy. Such an electron is localized in space while electrons in a uniform electron gas are spread out over the full system, thus are de-localized. Figure 4.2(a) shows that for a localized electron common exchange functionals give a poor description of the exact exchange energy.

Mapping the ELF in the CuO system shows that high ELF regions are located where the oxygen and copper electrons are commonly understood to be hybridizing (creating new states from the atomic oxygen and copper states), see Figure 4.3. Our analyse thus indicates that presently available DFT functionals make errors in this region, and not, as the common belief is, in the copper d-electron state. This is an important insight since many empirical schemes for correcting the errors DFT functionals make in these systems is based on the belief that the treatment of the d-electrons is at fault.

A functional for confined systems

By using the ELF as an indicator of the degree of confinement and use the exchange energy from the HO system in regions where the ELF is high, while using the AM05 (LAA) exchange in the rest of the system, we have the fundaments of a new functional. Since we do not have any correlation for the HO system, we construct our correlation so that it, together with the new exchange functional, reproduce the exact total exchange-correlation of surface jellium systems, in the same way as AM05[3] is constructed. The details of the construction of this Hao-Armiento-Mattsson (HAM) functional is described in Appendix B.

Just as the ordinary gradient corrected GGA type functionals, such as AM05 and PBE, the new HAM functional needs the density and the gradient of the density in order to extract a value for the exchange-correlation energy per particle. However, the HAM functional also needs the kinetic energy density and is thus classified as a meta-GGA. The implementation of meta-GGAs into DFT codes is feasible but substantially more elaborate than the implementation of a GGA functional. We have thus proceeded by applying the HAM functional as a post-correction on LDA results. In Figure 4.4 we show that the post-correction scheme we use reproduces the AM05 and PBE self-consistent results reasonably well. In essence this means that the LDA density compares well with the AM05 and PBE densities. In Figure 4.5 we show the result for the post-correction with the HAM functional. Indeed, the inclusion of confinement physics into the HAM functional does make the equilibrium volume smaller, and closer to the experimental value, for the CuO system. Further testing is needed to confirm that the HAM functional generally provides a consistently better or similar approximation for the exact exchange-correlation energy as existing functionals.

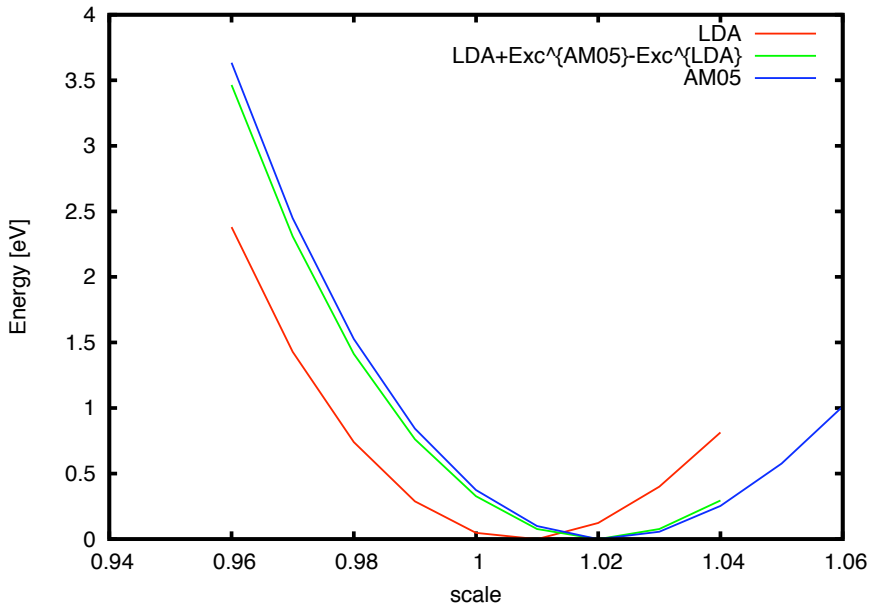

(a) Post-correction results (green) for AM05 on LDA, compared to self-consistent AM05 results (blue).

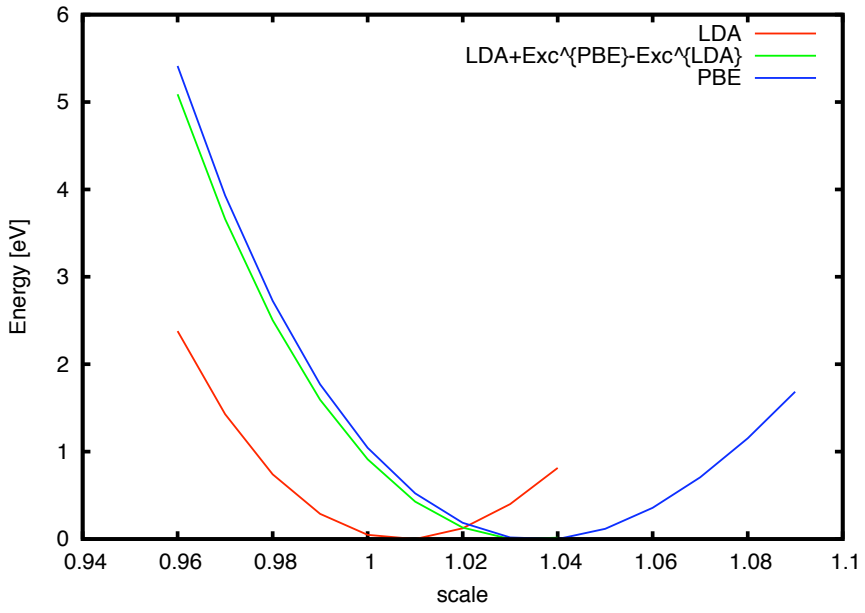

(b) Post-correction results (green) for PBE on LDA, compared to self-consistent PBE results (blue).

Figure 4.4. Test of the post-correction scheme we use for preliminary testing of the HAM functional, shown in Figure 4.5.

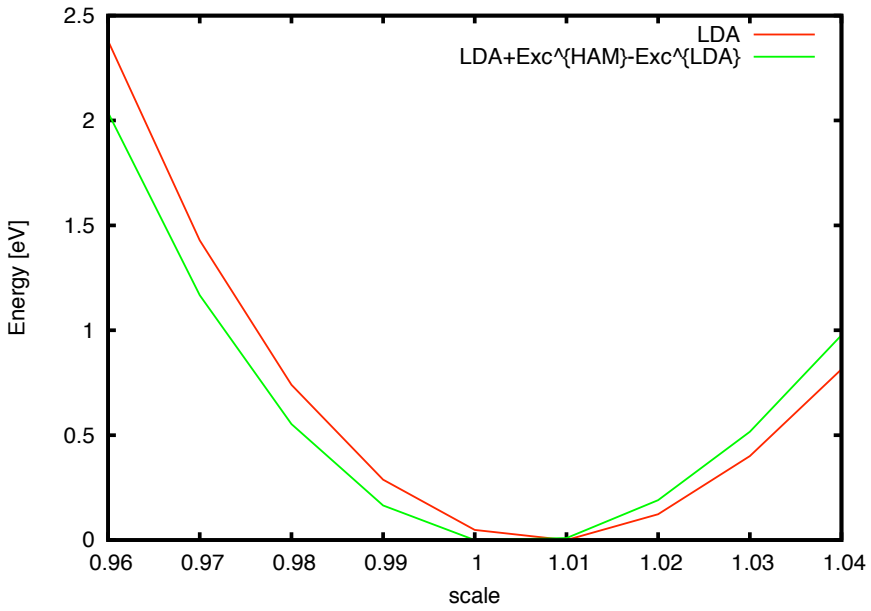

Figure 4.5. Post-correction results with the new HAM functional. Compared to LDA, AM05, and PBE the HAM functional correctly gives a smaller equilibrium volume for CuO.

Chapter 5

Summary and Conclusion

As the codes available for use in Engineering Sciences become more and more sophisticated, materials models used in these codes need to be increasingly accurate. Sandia scientists are at the forefront of DFT-based EOS construction, where experimental information is amended with information obtained in computational investigations, in order to achieve improved accuracy.

We have implemented a fully relativistic treatment based on the Dirac Equation into the LANL code RSPt and we have shown that such a treatment is imperative when calculating properties of materials containing actinides and/or lanthanides. The present standard treatment that only includes some of the relativistic terms is not accurate enough and can even give misleading results. Compared to calculations previously considered state of the art, the Dirac treatment gives a substantial change in equilibrium volume predictions for materials with large spin-orbit coupling. For actinide and lanthanide materials, a Dirac treatment is thus a fundamental requirement in any computational investigation, including those for DFT-based EOS construction.

For a full capability, a DFT functional capable of describing strongly correlated systems such as actinide materials need to be developed. Using the previously successful subsystem functional scheme developed by Mattsson *et.al.*, we have attempted to created such a functional. It is based on three model systems, the uniform electron gas, the surface jellium/Airy gas, and the Harmonic Oscillator Gas. The Harmonic Oscillator Gas is providing the necessary reference system for the strong correlation and localization occurring in actinides. Preliminary testing shows that the new Hao-Armiento-Mattsson (HAM) functional gives a trend towards improved results for the crystalline copper oxide test system we have chosen. During the work important insights have been gained. An example is that currently available functionals, contrary to common belief, make large errors in so called hybridization regions where electrons from different ions interact and form new states.

Together with the new understanding of functional issues, the Dirac implementation into the RSPt code will permit us to gain more fundamental understanding, both quantitatively and qualitatively, of materials of importance for Sandia and the rest of the Nuclear Weapons complex.

References

[1] The RSPt code. See http://www.rspt.net.

[2] R. Armiento and A. E. Mattsson. Subsystem functionals in density-functional theory: Investigating the exchange energy per particle. *Phys. Rev. B*, 66:165117, Oct 2002.

[3] R. Armiento and A. E. Mattsson. Functional designed to include surface effects in self-consistent density functional theory. *Phys. Rev. B*, 72:085108, Aug 2005.

[4] Peter E. Blöchl, O. Jepsen, and O. K. Andersen. Improved tetrahedron method for brillouin-zone integrations. *Phys. Rev. B*, 49:16223–16233, Jun 1994.

[5] Ram Devanathan, Laurent Van Brutzel, Alain Chartier, Christine Gueneau, Ann E. Mattsson, Veena Tikare, Timothy Bartel, Theodore Besmann, Marius Stan, and Paul Van Uffelen. Modeling and simulation of nuclear fuel materials. *Energy Environ. Sci.*, 3:1406–1426, 2010.

[6] R. M. Dreizler and E. K. U. Gross. *Density Functional Theory: An Approach to the Quantum Many-Body Problem*. Springer-Verlag, Berlin, 1990.

[7] G. W. Fernando, E. H. Sevilla, and Bernard R. Cooper. Theoretical study of relativistic effects in the electronic structure of pu. *Phys. Rev. B*, 61:12562–12565, May 2000.

[8] Sverre Froyen. Brillouin-zone integration by fourier quadrature: Special points for superlattice and supercell calculations. *Phys. Rev. B*, 39:3168–3172, Feb 1989.

[9] Philipp Haas, Fabien Tran, and Peter Blaha. Calculation of the lattice constant of solids with semilocal functionals. *Phys. Rev. B*, 79:085104, Feb 2009.

[10] Feng Hao, Rickard Armiento, and Ann E. Mattsson. Subsystem functionals and the missing ingredient of confinement physics in density functionals. *Phys. Rev. B*, 82:115103, Sep 2010.

[11] Feng Hao, Rickard Armiento, and Ann E. Mattsson. On the origins of the deficiencies of density functional theory exchange-correlation functionals for transition metal monoxides. Technical Report SAND2011-1553J, Sandia National Laboratories, 2011.

[12] P. Hohenberg and W. Kohn. Inhomogeneous electron gas. *Phys. Rev.*, 136:B864–B871, Nov 1964.

[13] M. D. Jones, J. C. Boettger, R. C. Albers, and D. J. Singh. Theoretical atomic volumes of the light actinides. *Phys. Rev. B*, 61:4644–4650, Feb 2000.

[14] M. D. Knudson and M. P. Desjarlais. Shock compression of quartz to 1.6 tpa: Redefining a pressure standard. *Phys. Rev. Lett.*, 103:225501, Nov 2009.

[15] D D Koelling and B N Harmon. A technique for relativistic spin-polarised calculations. *Journal of Physics C: Solid State Physics*, 10(16):3107, 1977.

[16] W. Kohn and L. J. Sham. Self-consistent equations including exchange and correlation effects. *Phys. Rev.*, 140:A1133–A1138, Nov 1965.

[17] Walter Kohn and Ann E. Mattsson. Edge electron gas. *Phys. Rev. Lett.*, 81:3487–3490, Oct 1998.

[18] Rudolph J. Magyar, Ann E. Mattsson, and Peter A. Schultz. Some practical considerations for density functional theory studies of chemistry at metal surfaces. In Thomas C. Allison, Orkid Coskuner, and Carlos A. González, editors, *Metallic Systems: A Quantum Chemist's Perspective*. CRC Press, Boca Raton, London, New York, 2011.

[19] Ann E. Mattsson. In pursuit of the "divine" functional. *Science*, 298(5594):759–760, 2002.

[20] Ann E. Mattsson and Rickard Armiento. The subsystem functional scheme: The Armiento-Mattsson 2005 (AM05) functional and beyond. *International Journal of Quantum Chemistry*, 110(12):2274–2282, 2010.

[21] Ann E. Mattsson, Rickard Armiento, Joachim Paier, Georg Kresse, John M. Wills, and Thomas R. Mattsson. The AM05 density functional applied to solids. *The Journal of Chemical Physics*, 128(8):084714, 2008.

[22] M. Methfessel and A. T. Paxton. High-precision sampling for brillouin-zone integration in metals. *Phys. Rev. B*, 40:3616–3621, Aug 1989.

[23] L. Nordström, J. M. Wills, P. H. Andersson, P. Söderlind, and O. Eriksson. Spin-orbit coupling in the actinide elements: a critical evaluation of theoretical equilibrium volumes. *Phys. Rev. B*, 63:035103, Dec 2000.

[24] John P. Perdew, Kieron Burke, and Matthias Ernzerhof. Generalized gradient approximation made simple. *Phys. Rev. Lett.*, 77:3865–3868, Oct 1996.

[25] John P. Perdew and Yue Wang. Accurate and simple analytic representation of the electron-gas correlation energy. *Phys. Rev. B*, 45:13244–13249, Jun 1992.

[26] Seth Root, Rudolph J. Magyar, John H. Carpenter, David L. Hanson, and Thomas R. Mattsson. Shock compression of a fifth period element: Liquid xenon to 840 GPa. *Phys. Rev. Lett.*, 105:085501, Aug 2010.

[27] J. J. Sakurai. *Advanced Quantum Mechanics*. Addison-Wesley Publishing Company, 1967.

[28] Avram Sidi. Some aspects of two-point pade approximants. *J. Comp. Appl. Math.*, 6:9–17, 1980.

[29] P. Söderlind, O. Eriksson, B. Johansson, and J. M. Wills. Electronic properties of f-electron metals using the generalized gradient approximation. *Phys. Rev. B*, 50:7291–7294, Sep 1994.

[30] J. M. Wills, O. Eriksson, M. Alouani, and D. L. Price. Full potential LMTO: Total energy and force calculations. In H. Dreysse, editor, *Electronic Structure and Physical Properties of Solids: The Uses of the LMTO Method*, volume 535 of *Lecture Notes in Physics*. Springer-Verlag, Berlin, 2000.

[31] John M. Wills, Torey Semi, and Ann E. Mattsson. The dirac equation and its implications for density functional theory based calculations of materials containing heavy elements. Technical Report SAND2011-7521J, Sandia National Laboratories, 2011.

Appendix A

Implementational details for DiracRSPt: The transition to full Dirac bases in the framework of RSPt

An electronic structure method capable of performing fully relativistic electronic structure calculations has been developed within the framework of the full potential electronic structure code RSPt.[1] The development necessary to accomplish this includes the the calculation of the Dirac spinors around atom sites and in the interstitial, the construction of a Hamiltonian and overlap matrix, and the construction of the charge density. In this Appendix we discuss these changes in relation to the already existing implementation of the RSPt code, described in Reference 30.

A.1 Introduction: the transition from RSPt to Dirac

In the discussion that follows, Rydberg units are used; *i.e.* $\hbar = 1$, the square of the electron charge $e^2 = 2$, and twice the electron mass $2m = 1$. The designation "RSPt"[1] refers to the scalar relativistic all electron electronic structure code that provides the framework for DiracRSPt, the code discussed here.

Indexing

In RSPt, indexing is by ℓ or ℓm, with limits $\ell \in [0, \ell_m]$.[30] The transition to Dirac indexing is accomplished by

$$\begin{aligned} k_p &\in [0, 2\ell_m] \\ \ell &= \left[\frac{k_p+1}{2}\right] \\ \kappa &= (-)^{k+1}\left(\left[\frac{k_p}{2}\right]+1\right) \\ 2j &= 2\left[\frac{k_p}{2}\right]+1 \end{aligned}$$

To count $k_p m = \ell j m$ in the full list: $k_p \in [0, 2\ell_m], 2m_{k_p} \in [-2[k_p/2]-1, 2[k_p/2]+1, 2]$

$$\begin{aligned} \sum_{i=0}^{[k_p/2]-1} 4(i+1) &+ 2\mathrm{mod}(k_p,2)([k_p/2]+1) + jm + 1 \\ &= 2[k_p/2]([k_p/2]+1) + 2(k_p - 2[k_p/2])([k_p/2]+1) + jm + 1 \\ &= 2(k_p - [k_p/2])([k_p/2]+1) + jm + 1 \\ jm &\equiv (j+m) \in [0, 2\lfloor k_p/2 \rfloor + 1] \end{aligned}$$

Somewhat more cumbersome that the simple $\ell^2 + \ell + m + 1$, but not too bad.

The transition to Dirac bases

A LMTO basis function is an *envelope* function, centered on a site τ in a unit cell,

$$\mathcal{K}_i(\mu; k, r) \equiv \sum_R \exp(ik \cdot R)\mathcal{K}_i(\mu; |r - \tau - R|)\mathcal{A}_i(r - \tau - R) \tag{A.1}$$

joined to a basis of spherical waves,

$$\Phi_{\mathcal{K}}(r - \tau') = \sum_j U_j^T(r - \tau')\mathrm{S}_{ji}^{\tau'-\tau}(\mu; k) \tag{A.2}$$

centered on each atomic site τ' in a unit cell, calculated from a wave equation appropriate to the spherically symmetric component of the DFT potential in a sphere (the *muffin-tin sphere*) centered on that site. In a scalar relativistic (SR) calculation, the

envelope functions are Hankel or Neumann functions (depending on the sign of the kinetic energy μ^2), with separable angular- and spin-angular-momentum components $\mathcal{Y}_{\ell m}(r)\chi_{m_s}$. In the fully relativistic calculation (Dirac) developed here, the envelope functions are constant potential, positive energy Dirac spinors, with Hankel or Neuman upper components and kinetic energy $E-mc^2 = \sqrt{\mu^2+(mc)^2}-mc^2$, and angular momentum components $\langle r|\kappa m\rangle$ for the upper component and $\langle r|-\kappa m\rangle$ for the lower component, where $\langle r|\kappa m\rangle = \sum_{m_\ell m_s} \left(\ell(\kappa)\ m_\ell\ {}^1\!/_2\ m_s|\ell(\kappa)\ {}^1\!/_2\ j(\kappa)\ m\right) \mathcal{Y}_{\ell m_\ell}\chi_{m_s}$.

The tasks of a DFT based electronic structure method are to create a basis, calculate the Hamiltonian and overlap matrix in this basis, create an electron density from the resulting eigenvectors, and use this density together with calculated eigenvalues to calculate an output potential and total energy. The change from SR to Dirac bases modifies all these tasks.

Bases in muffin tin spheres

The "L" in LMTO stands for "linearized", so named because the LMTO basis set was originally derived from a first-order expansion around band energies in the non-linear KKR method. In RSPt, as in many other codes, the concept of linearization is largely irrelevant; but the basis still consists of numerical scalar-Dirac or Dirac radial functions and their derivatives with respect to one-electron energy. Let $G_\ell = rg_\ell$, $\Phi_\ell = r\phi_\ell$. The scalar-Dirac equation of Harmon and Koelling for the radial function $g(r) = G(r)/r$ and the subsidiary function $\Phi(r) = g'(r)/2Mrc$ with $M \equiv m + (e - V(r))/2c^2$ is

$$\frac{d}{dr}\begin{pmatrix} G_\ell \\ \Phi_\ell \end{pmatrix} = \begin{pmatrix} \frac{1}{r} & 2Mc \\ \frac{\ell(\ell+1)}{2Mcr^2} - \frac{(e-V)}{c} & -\frac{1}{r} \end{pmatrix} \begin{pmatrix} G_\ell \\ \Phi_\ell \end{pmatrix}. \tag{A.3}$$

with the boundary condition at the origin

$$\begin{aligned} G &\rightarrow r^\mu, \quad \mu = \sqrt{\ell(\ell+1)+1-(Ze^2/c)^2},\ r \rightarrow 0 \\ \frac{\Phi}{G} &\rightarrow \frac{\mu-1}{Ze^2/c} \end{aligned}$$

Equation (A.3) is similar in structure to the Dirac equation for the radial basis function

$$\psi_{\kappa m}(r) = \frac{1}{r}\begin{pmatrix} G_\kappa(r) \\ -iF_\kappa(r)\sigma_r \end{pmatrix} |\kappa m\rangle$$

The radial Dirac equation for $\psi_{\kappa m}$ is

$$\frac{d}{dr}\begin{pmatrix} G_\kappa \\ F_\kappa \end{pmatrix} = \begin{pmatrix} -\frac{\kappa}{r} & 2Mc \\ -\frac{1}{c}(e-V) & \frac{\kappa}{r} \end{pmatrix} \begin{pmatrix} G_\kappa \\ F_\kappa \end{pmatrix} \tag{A.4}$$

where $e \equiv E - mc^2$, E including the rest energy. The boundary condition at the origin, if $V(r) \to -Ze^2/r$, is

$$\begin{aligned} G_\kappa &\to r^\mu, \quad mu = \sqrt{\kappa^2 - (Z\alpha)^2} \\ \frac{F_\kappa}{G_\kappa} &\to \frac{\mu + \kappa}{Z\alpha} \end{aligned}$$

The similarity between equations (A.3) and (A.4) allows ready conversion from scalar-relativistic to full Dirac bases.

Radial matrix elements

The structure of the matrix elements of the Hamiltonian and overlap matrices is similar between scalar relativistic and Dirac bases, with one exception. The spin-orbit interaction is built into the Dirac spinors, therefore no matrix elements of a spin-orbit interaction, used in scalar relativistic treatments to include the spin-orbit interaction variationally, are necessary in the full Dirac treatment.

Connecting the interstitial to muffin-tins: structure constants

The coefficients S in equation (A.2), connecting the envelope function in the interstitial to muffin-tin basis functions, are known as structure constants. Because the momentum operator is translationally invariant, a spherical Hankel function, centered on point r, is a finite solution to the Helmholtz equation about any other site r', and therefore has an expansion in Bessel functions about r'. Equation (A.2) embodies this observation which determines the structure constants for any given atomic site. In reciprocal space, the part of the structure constant that expands the scalar-relativistic envelope function about a site other than its parent site ($\tau' \neq \tau$) is given by

$$\begin{aligned} &B_{L',L}(\boldsymbol{\tau} - \boldsymbol{\tau}, \mu, k)\delta(m_s, m_s') \qquad \text{(A.5)} \\ &= 4\pi \sum_{L''} (-)^{(-\ell'+\ell-\ell'')/2} (\mu^2)^{(\ell'+\ell-\ell'')/2} \sqrt{2\ell'' + \frac{1}{4\pi}} \mathcal{G}(L', L, L'') D_{L''}(\tau' - \tau; \kappa; k)\delta(m_s, m_s') \end{aligned}$$

In equation (A.5), L is a composite index representing ℓ and m_ℓ, D_L is a Bloch sum of Hankel function spherical waves, and $\mathcal{G}$ is an angular matrix element:

$$\begin{aligned}
\mathcal{G}(L', L, L'') &\equiv \big(\mathcal{Y}_{L'}\big|\mathcal{C}_{L''}\big|\mathcal{Y}_L\big) \\
&= (-)^{\ell'-m'}(i)^{\ell-\ell'+\ell_h}\begin{pmatrix} \ell' & \ell_h & \ell \\ -m' & m_h & m \end{pmatrix}\big(\ell'\big\|C(\ell_h)\big\|\ell\big) \\
\big(\ell'\big\|C(\ell_h)\big\|\ell\big) &= \sqrt{(2\ell+1)(2\ell'+1)}(-)^{\ell'}\begin{pmatrix} \ell' & \ell_h & \ell \\ 0 & 0 & 0 \end{pmatrix}
\end{aligned} \tag{A.6}$$

For a full Dirac basis, the envelope functions are spinors, Hankel solution to the spherical Dirac equation for a constant potential. Because the upper component of this spinor is a simple transformation of the scalar-relativistic envelope function *via* vector coupling coefficients, the structure constant analogous to equation (A.5) for the full Dirac envelope function is simply the same transform applied to the rows and columns of equation (A.5):

$$\begin{aligned}
&B_{\kappa'm',\kappa m}(\boldsymbol{\tau}-\boldsymbol{\tau}, \mu, k) \qquad\qquad (A.7)\\
&\quad = 4\pi\sum_{L''}(-)^{(-\ell'+\ell-\ell'')/2}(\mu^2)^{(\ell'+\ell-\ell'')/2}\sqrt{2\ell''+\frac{1}{4\pi}}\mathcal{G}(\kappa'm', \kappa m, L'')D_{L''}(\tau'-\tau;\kappa;k)
\end{aligned}$$

$$\begin{aligned}
\mathcal{G}(\kappa'm', \kappa m, L'') &\equiv \big(\kappa'm'\big|\mathcal{C}_{L''}\delta(m'_s, m_s)\big|\kappa m\big) \\
&= (-)^{\ell'-m'}(i)^{\ell-\ell'+\ell_h}\begin{pmatrix} \ell' & \ell_h & \ell \\ -m' & m_h & m \end{pmatrix}\big(\kappa'\big\|C(\ell_h)\big\|\kappa\big) \\
\big(\ell'{}^1\!/_2 j'\big\|\mathcal{C}(\ell'')\big\|\ell{}^1\!/_2 j\big) &= (-)^{\ell'+1/2+j+\ell''}\sqrt{(2j'+1)(2j+1)}\begin{Bmatrix} \ell' & j' & 1/2 \\ j & \ell & \ell'' \end{Bmatrix}\big(\ell'\big\|\mathcal{C}(\ell'')\big\|\ell\big)
\end{aligned} \tag{A.8}$$

A.2 Matrix Elements

The Hamiltonian and overlap matrix elements are used to obtain eigenvalues and eigenvectors with which to construct the electron density, potential, and total energy. The steps in constructing these matrices, in this formalism are: muffin tin spherical Hamiltonian and overlap, and the muffin-tin non-spherical potential, the interstitial kinetic energy and overlap, and the interstitial potential. In RSPt, a spin-orbit Hamiltonian contribution is added. In the transition to Dirac, apart from the expanded structure constants, the essential differences occur in the three interstitial contributions and in the contribution from the non-spherical muffin-tin potential.

The non-spherical potential in the muffin-tin

This section is limited to a discussion of spin-independent potentials. The potential in a muffin tin sphere takes the form

$$\begin{aligned} V_{ns}(r_\tau) &= \sum_h v(ht;r_\tau) D_{ht}(\hat{r}_\tau) \\ D_{ht}(r_\tau) &= \sum_{m_h} \alpha(ht;m_h) \mathcal{C}_{\ell_h m_h}(\hat{r_\tau} \end{aligned} \tag{A.9}$$

where h labels symmetric harmonics D_h of the symmetry group surrounding the atomic site at τ. The contribution of V_{ns} to the Hamiltonian matrix consists of a sum of radial matrix elements of v_h times angular matrix elements of D_h. These last are symmetric sums of the scaled Gaunt coefficients defined in equations (A.6) and (A.8). For the Dirac case,

$$\big(\kappa' m' \big| D_h \big| \kappa m\big) = \sum_{m_h} \alpha(ht;m_h) \mathcal{G}(\kappa m, \kappa' m', \ell_h m_h) \tag{A.10}$$

The interstitial kinetic energy and overlap

The interstitial kinetic energy and overlap matrices are obtained by integrating over the surface of the muffin-tin spheres. The difference between scalar relativistic and Dirac bases is to be found in the continuity conditions imposed by the corresponding equations. With Dirac bases, $(\mathcal{H}_D - mc^2)\mathcal{K} = (c\alpha \cdot p + (\beta - 1)mc^2)\mathcal{K} = (\mu^2/2M_\mu)\mathcal{K}$ in the interstitial.

If $e = E - mc^2 = \mu^2/2M(\mu)$ with $2M(\mu) \equiv m(1 + \sqrt{1 + (\mu/mc)^2})$,

$$\begin{aligned} (e_b - e_a) \int_{\mathcal{I}} \psi_a^\dagger \psi_b &= \int_{\mathcal{I}} \Big(\psi_a^\dagger \mathcal{H}_D \psi_b - \big(\mathcal{H}_D \psi_a\big)^\dagger \psi_b \Big) \\ &= c\boldsymbol{\alpha}_{\mu\nu} \cdot \int_{\mathcal{I}} \big(\psi_{a\mu}^\star \mathbf{p} \psi_{b\nu} - (\mathbf{p}\psi_{a\mu})^\star \psi_{b\nu} \big) \\ &= -ic\boldsymbol{\alpha}_{\mu\nu} \cdot \int_{\mathcal{I}} \boldsymbol{\nabla} \Big(\psi_{a\mu}^\star \psi_{b\nu} \Big) \\ &= ic \sum_\tau S_t^2 \int d\Omega \psi_a^\dagger \boldsymbol{\alpha} \cdot \hat{\mathbf{r}} \psi_b \end{aligned}$$

To make equation (A.2) explicit, the envelope function for basis a, centered on τ_a, expanded on the sphere at τ, is

$$\psi_a(S_\tau) = \sum_{\kappa m} \mathrm{K}_{\kappa m}(\mu_a, S_\tau) \mathrm{S}_{\tau\kappa m, \tau_a \kappa_a m_a}(\mu_a, k) \tag{A.11}$$

where K is a row vector of dirac spinors:

$$\mathrm{K}_{\kappa m}(\mu, r) = \begin{pmatrix} \mathcal{K}_{\kappa m}(\mu, r) & \mathcal{J}_{\kappa m}(\mu, r) \end{pmatrix}$$

The overlap matrix element becomes

$$\begin{aligned} &(e_b - e_a) \int_{\mathcal{I}} \psi_a^\dagger \psi_b \\ &= ic \sum_\tau S_\tau^2 \sum_{\kappa m} \mathrm{S}^\dagger_{\tau\kappa m, \tau_a \kappa_a m_a}(\mu_a, \mathbf{k}) \int d\Omega \mathrm{K}^\dagger_{\kappa m}(\mu_a, S_\tau) \boldsymbol{\alpha} \cdot \hat{\mathbf{r}} \mathrm{K}_{\kappa m}(\mu_b, S_\tau) \mathrm{S}_{\tau\kappa' m', \tau_b \kappa_b m_b}(\mu_b, \mathbf{k}) \end{aligned}$$

After some manipulation, this reduces to

$$\int_{\mathcal{I}} \psi_a^\dagger \psi_b = \sqrt{\frac{1}{2M_a} \frac{1}{2M_b}} \sum_{\tau\kappa m} \mathrm{S}^\dagger_{\tau\kappa m, \tau_a \kappa_a m_a}(\mu_a, \mathbf{k}) \Big(w_{\kappa m}(t; a, b) + \frac{S_\tau^2 W_0}{e_b - e_a} \Big) \mathrm{S}_{\tau\kappa m, \tau_b \kappa_b m_b}(\mu_b, \mathbf{k}) \tag{A.12}$$

where

$$\bar{w}_{\kappa m}(t; a, b) \equiv S_t^2 \left(\sqrt{2M_a} W \left(\mathrm{K}^\dagger_{\kappa m}(\mu_a, S_\tau), \mathrm{K}_{\kappa m}(\mu_b, S_\tau) \right) \sqrt{2M_b} - W_0 \right) / (e_b - e_a) \tag{A.13}$$

$$W(f, g) \equiv f^{(1)} c g^{(2)} - c f^{(2)} g^{(1)} \tag{A.14}$$

$$S_t^2 W_0 \equiv \begin{pmatrix} 0 & 1 \\ -1 & 0 \end{pmatrix}$$

When $e_a = e_b$, equation (A.13) vanishes and the remainder is a difference of structure constants divided by a difference of energies, which becomes the derivative $\partial S / \partial e$ as $e_a \to e_b$. The full Hamiltonian is explicitly symmetrized, so that the kinetic energy is obtained from the overlap through

$$T_{ab} = \frac{1}{2} \int \left(\psi_a^\dagger H_D \psi_b + (H_D \psi_a)^\dagger \psi_b \right) = \frac{1}{2} (e_a + e_b) \int \psi_a^\dagger \psi_b$$

The interstitial potential matrix

In the muffin tins, where the radial gradients around a site are large, and the evolution is from spherical symmetry, the one-electron potential is expressed in spherical waves, as in equation (A.9). The muffin-tins and interstitial are evaluated separately, so that to obtain matrix elements of the interstitial potential, any potential that matches the true potential in the interstitial may be used. In the region between the spheres, the

interstitial, the potential is "nearly" constant, so the freedom to choose this alternate potential may be used to obtain a rapidly convergent Fourier series

$$\tilde{V}(r) = \sum_{\mathcal{S}} \tilde{v}(\mathcal{S}) \sum_{g \in \mathcal{S}} \exp(ig \cdot r) \tag{A.15}$$

$$\left(\tilde{V}(r) - V(r)\right) \Theta(r \in \mathcal{I}) = 0 \tag{A.16}$$

The sums in equation(A.15) are over stars $\mathcal{S}$ of the reciprocal lattice and vectors g belonging to each star, respectively.

In practice, the "pseudizing" is accomplished by choosing pseudo basis functions with rapidly convergent Fourier series and matching the true basis functions in the interstitial. The density in the interstitial thus matches the true density, and a similar construction of a pseudo density giving the correct Coulomb potential in the interstitial results in a "pseudo-potential" that agrees with the true potential in the interstitial.

In the scalar-relativistic RSPt, the pseudo-bases are obtained by constructing solutions to

$$\begin{aligned} \left(\nabla^2 + \mu^2\right) \tilde{\psi}_{\tau\ell}(r_\tau) \mathcal{Y}_{\ell m}(r_\tau) &= -c_{\tau\ell} x^\ell \left(1 - x^2\right)^{n_{\tau\ell}} \mathcal{Y}_{\ell m}(r_\tau) && \text{(A.17)} \\ x &\equiv \frac{r_\tau}{S_\tau} \\ \tilde{\psi}_{\tau\ell}(S_\tau) &= \mathcal{K}_\ell(\mu, S_\tau) && \text{(A.18)} \end{aligned}$$

The boundary condition equation (A.18) is satisfied by choosing the constant $c_{\tau\ell}$. Equation (A.17) has a closed form solution, but the solution itself, given that it exists, is irrelevant since the Fourier transform is obtained from the equation (A.17) through

$$\begin{aligned} \int \exp(-i(K \cdot r))\tilde{\psi} &= -\frac{1}{K^2 - \mu^2} \int \left((\nabla^2 - \mu^2) \exp(-iK \cdot r)\right) \tilde{\psi} \\ &= -\frac{1}{K^2 - \mu^2} \int \exp(-iK \cdot r) \left((\nabla^2 - \mu^2)\tilde{\psi}\right) \end{aligned}$$

where $K = k + g$. The fourier transform of the scalar-relativistic envelope function $\mathcal{K}_{\ell m}\chi_{m_s}$ centered on site τ is

$$\tilde{\mathcal{K}}_{\ell m}(\mu, S_\tau, K) = \frac{4\pi}{V_c} \frac{\exp(-iK \cdot \tau)}{K^2 - \mu^2} K^\ell Y_{\ell m}(K) \frac{\mathcal{J}_N(K, S_\tau)}{\mathcal{J}_N(\mu, S_\tau)} \tag{A.19}$$

where N is a constant greater than $\ell_m + 1$.

A similar construction could be made for the Dirac envelope, but since upper and lower components have radial dependence $\mathcal{K}_\ell$ and $\mathcal{K}_{\ell\pm1}$, the functional form equation(A.19), transformed according to

$$\big(K\big|\kappa m\big) = \sum_{m_\ell m_s} \big(\ell m_\ell m_s\big|\kappa m\big) Y_{\ell m_\ell}(K)\chi_{m_s} \tag{A.20}$$

Appendix B

Details of an exchange-correlation functional for confined systems

B.1 Kinetic Energy density of HO gas

For electron gas confined in one dimension, the normalized eigenfunctions of the KS equation is:

$$\Psi_\nu(\mathbf{r}) = \frac{1}{A^{1/2}} e^{i(k_x x + k_y y)} \phi_j(z) \tag{B.1}$$

Thus, the kinetic energy density of the electron gas reads,

$$\tau(\mathbf{r}) = \sum_\nu |\nabla \Psi_\nu(\mathbf{r})|^2 = \sum_j \left[\frac{|\mu - \epsilon_j|^2}{2\pi} \phi_j^2(z) + \frac{|\mu - \epsilon_j|}{2\pi} \phi_j'^2(z) \right] \tag{B.2}$$

For the HO gas, let $\bar{z} = z/l$,

$$\phi_j(z) = \tilde{\phi}_j(\bar{z})/l^{1/2} \tag{B.3}$$

$$\tilde{\phi}_j(\bar{z}) = \left(\frac{1}{\sqrt{\pi} 2^j j!} \right)^{\frac{1}{2}} \mathrm{H}_j(\bar{z}) e^{-\bar{z}^2/2} \tag{B.4}$$

$$\epsilon_j = \frac{1}{l^2}(j + 1/2) \tag{B.5}$$

Take derivative of $\phi(z)$,

$$\phi_j'(z) = \tilde{\phi}_j'(\bar{z})/l^{3/2} \tag{B.6}$$

$$\tilde{\phi}_j'(\bar{z}) = \left(\sqrt{\frac{j}{2}} \tilde{\phi}_{j-1}(\bar{z}) - \sqrt{\frac{j+1}{2}} \tilde{\phi}_{j+1}(\bar{z}) \right) \tag{B.7}$$

and substitue above equations in Eq. B.2, the kinetic energy density(dimensionless) of the HO is:

$$(l^5 \tau(\bar{z})) = \frac{1}{2\pi} \sum_{j=0}^{N} \left[(\alpha - j)^2 \tilde{\phi}_j^2(\bar{z}) + (\alpha - j) \tilde{\phi}_j'^2(\bar{z}) \right] \tag{B.8}$$

B.2 parameterization of the exchange energy per particle for HO gas

We assume the exchange energy per particle of the HO gas ϵ_x could be expressed in the following form:

$$\epsilon_x(\mathbf{r}) = \epsilon_x^{LDA}(n(\mathbf{r}))F_x(s(\mathbf{r}), q(\mathbf{r})) \tag{B.9}$$

There are two steps to find the anaytical form of the enhancement factor $F_x(s(\mathbf{r}), q(\mathbf{r}))$. In the HO gas, ϵ_x is a function of α and $\bar{z}$. First, we need to know the value of α and $\bar{z}$ from the local density information s and q. Also we need to have an analytical expression of the $F_x(\alpha, \bar{z})$. As shown in previous studies, the confinement physics mainly appears for systems with $\alpha < 1$, therefore, for simplicity, we will focus on these systems. If $\alpha < 1$,

$$(l^3 n(\bar{z})) = \frac{1}{\pi^{3/2}} e^{-\bar{z}^2} \alpha, \tag{B.10}$$

thus, we can derive the expression for s and q as following:

$$s = \frac{|\nabla n|}{2(3\pi^2)^{1/3} n^{4/3}} = \frac{|2\bar{z}|}{2(3\pi^{1/2}\alpha e^{-\bar{z}^2})^{1/3}} \tag{B.11}$$

$$q = \frac{\nabla^2 n}{4(3\pi^2)^{2/3} n^{5/3}} = \frac{4\bar{z}^2 - 2}{4(3\pi^{1/2}\alpha e^{-\bar{z}^2})^{2/3}} \tag{B.12}$$

Solve above equations, the expression of α and $\bar{z}$ may be written as,

$$\alpha = \left[\frac{1}{2(s^2 - q)}\right]^{3/2} / (3\pi^{1/2} e^{-\frac{s^2}{2(s^2-q)}}) \tag{B.13}$$

$$\bar{z}^2 = \frac{s^2}{2(s^2 - q)} \tag{B.14}$$

For $\alpha < 2$, The density took the following form:

$$(l^3 n(\bar{z})) = \frac{1}{\pi^{3/2}} e^{-\bar{z}^2} [\alpha + 2(\alpha - 1)\bar{z}^2], \tag{B.15}$$

So in such a case, the s and q will be:

$$s = \frac{|\nabla n|}{2(3\pi^2)^{1/3} n^{4/3}} = \frac{|(\alpha - 2)\bar{z} - 2(\alpha - 1)\bar{z}^3|}{(3\pi^{1/2} e^{-\bar{z}^2})^{1/3} [\alpha + 2(\alpha - 1)\bar{z}^2]^{4/3}} \tag{B.16}$$

$$q = \frac{\nabla^2 n}{4(3\pi^2)^{2/3} n^{5/3}} = \frac{2(\alpha - 1)\bar{z}^4 + (-4\alpha + 5)\bar{z}^2 + \alpha/2 - 1}{(3\pi^{1/2} e^{-\bar{z}^2})^{2/3} [\alpha + 2(\alpha - 1)\bar{z}^2]^{5/3}} \tag{B.17}$$

Another way to derive α and $\bar{z}$ is via dimensionless gradient s and the dimensionless kinetic energy t, which we defined as following:

$$t = \frac{\tau}{\tau^{unif}} = \frac{\tau}{(3/10)(3\pi^2)^{2/3}n^{5/3}} \tag{B.18}$$

For the HO with $\alpha < 1$,

$$t = \frac{5}{3}\frac{\alpha + \bar{z}^2}{(3\pi^{1/2}\alpha e^{-\bar{z}^2})^{2/3}} \tag{B.19}$$

Combined with the Eq.(B.11), the α and $\bar{z}^2$ could be solved as function of s and t:

$$\bar{z}^2 = \frac{1}{2}W\left[18\pi(\frac{3}{5}t - s^2)^2 s^2\right] \tag{B.20}$$

$$\alpha = \bar{z}^2\left(\frac{3}{5}\frac{t}{s^2} - 1\right) \tag{B.21}$$

where $W(x)$ is the Lambert W function.

Next, we are trying to derive the anaytical form of the exchange energy per particle of the HO gas for $\alpha < 1$.

$$\begin{aligned}(l\epsilon_x(\bar{z})) &= -\frac{1}{2\pi^2(l^3 n(\bar{z}))}\int d\bar{z}' e^{-(\bar{z}^2+\bar{z}'^2)}(\Delta\bar{z})^{-3} g(\sqrt{2\alpha}\Delta\bar{z}, \sqrt{2\alpha}\Delta\bar{z}) \\ &= -\frac{1}{\sqrt{\pi}}\int_{-\infty}^{\infty} d\bar{z}' e^{-\bar{z}'^2}(\Delta\bar{z})^{-1}\left[1/2 - \frac{I_1(2\sqrt{2\alpha}\Delta\bar{z})}{2\sqrt{2\alpha}\Delta\bar{z}} + \frac{L_1(2\sqrt{2\alpha}\Delta\bar{z})}{2\sqrt{2\alpha}\Delta\bar{z}}\right]\end{aligned} \tag{B.22}$$

Let $x = |\bar{z}' - \bar{z}|$, above integration now takes the form:

$$(l\epsilon_x(\bar{z})) = -\frac{1}{\sqrt{\pi}}\int_0^{\infty} dx\frac{1}{x}\left[1/2 - \frac{I_1(2\sqrt{2\alpha}x)}{2\sqrt{2\alpha}x} + \frac{L_1(2\sqrt{2\alpha}x)}{2\sqrt{2\alpha}x}\right]\left[e^{-(\bar{z}+x)^2} + e^{-(\bar{z}-x)^2}\right] \tag{B.23}$$

In the following we derive the asymptotic behavior for $l\epsilon_x(\bar{z})$ when $\bar{z} \to +\infty$. First we have two approximations:

$$\begin{aligned}\int_0^{\infty} dx\frac{1}{x}e^{-(x-\bar{z})^2} &\approx \frac{\sqrt{\pi}}{\bar{z}}(\bar{z} \to +\infty) \\ \int_0^{\infty} dx\frac{1}{x^2}e^{-(x-\bar{z})^2} &\approx \frac{\sqrt{\pi}}{\bar{z}^2}(\bar{z} \to +\infty) \\ \int_0^{\infty} dx\frac{1}{x^4}e^{-(x-\bar{z})^2} &\approx \frac{\sqrt{\pi}}{\bar{z}^4}(\bar{z} \to +\infty)\end{aligned} \tag{B.24}$$

Also notice that,

$$L_1(2\sqrt{2\alpha}x) - I_1(2\sqrt{2\alpha}x) \approx -\frac{2}{\pi} + \frac{1}{4\pi\alpha x^2}(x \to +\infty) \tag{B.25}$$

then in the limit of $\bar{z} \to +\infty$, the Eq. (B.23) now becomes:

$$\begin{aligned}(l\epsilon_x(\bar{z})) &= -\frac{1}{\sqrt{\pi}}\int_0^\infty dx\frac{1}{x}(1/2 - \frac{1}{\pi\sqrt{2\alpha}x} + \frac{1}{8\pi\alpha\sqrt{2\alpha}x^3})e^{-(x-\bar{z})^2} \\ &= -\frac{1}{2\bar{z}} + \frac{1}{\pi\sqrt{2\alpha}\bar{z}^2} - \frac{1}{8\pi\alpha\sqrt{2\alpha}\bar{z}^4}\end{aligned} \tag{B.26}$$

Next we derive the limit of $l\epsilon_x(\bar{z})$ for $\bar{z} \to 0$. Consider $\bar{z}$ is small, and expand $e^{-(x+\bar{z})^2} + e^{-(x-\bar{z})^2}$ around x, we have $e^{-(x+\bar{z})^2} + e^{-(x-\bar{z})^2} \approx e^{-x^2}[2 + (4x^2 - 2)\bar{z}^2 + (\frac{4}{3}x^4 - 4x^2 + 1)\bar{z}^4 + (\frac{8}{45}x^6 - \frac{4}{3}x^4 + 2x^2 - \frac{1}{3})\bar{z}^6]$. Let

$$\begin{aligned}A &= -\frac{1}{\sqrt{\pi}}\int_0^\infty dx\frac{1}{x}\left[1/2 - \frac{I_1(x)}{x} + \frac{L_1(x)}{x}\right]e^{-\frac{x^2}{8\alpha}} \\ &= \frac{1-\gamma-\ln(-2\alpha)-\Gamma(0,-2\alpha)}{4\sqrt{\pi}} - \frac{2\sqrt{2\alpha}}{3\pi} + \frac{1-e^{2\alpha}}{8\sqrt{\pi}\alpha} - \frac{8\sqrt{2}\alpha^{3/2}{}_2F_2\left(1,\frac{3}{2};\frac{5}{2},\frac{7}{2};2\alpha\right)}{45\pi} \\ B &= -\frac{1}{\sqrt{\pi}}\int_0^\infty dx\frac{1}{x}\left[1/2 - \frac{I_1(x)}{x} + \frac{L_1(x)}{x}\right]x^2e^{-\frac{x^2}{8\alpha}} \\ &= \frac{e^{2\alpha}\mathrm{erfc}(\sqrt{2\alpha}) - 1 - 2\alpha}{\sqrt{\pi}} + \frac{2\sqrt{2\alpha}}{\pi} \\ C &= -\frac{1}{\sqrt{\pi}}\int_0^\infty dx\frac{1}{x}\left[1/2 - \frac{I_1(x)}{x} + \frac{L_1(x)}{x}\right]x^4e^{-\frac{x^2}{8\alpha}} \\ &= \frac{16\alpha^2[e^{2\alpha}\mathrm{erfc}(\sqrt{2\alpha}) - 1]}{\sqrt{\pi}} \\ D &= -\frac{1}{\sqrt{\pi}}\int_0^\infty dx\frac{1}{x}\left[1/2 - \frac{I_1(x)}{x} + \frac{L_1(x)}{x}\right]x^6e^{-\frac{x^2}{8\alpha}} \\ &= \frac{128\alpha^3[2(1+\alpha)e^{2\alpha}\mathrm{erfc}(\sqrt{2\alpha}) - \sqrt{2\alpha/\pi} - 2]}{\sqrt{\pi}}\end{aligned} \tag{B.27}$$

where γ is the Euler's constant, $\Gamma(0,-2\alpha)$ is an upper incomplete gamma function, ${}_2F_2\left(1,\frac{3}{2};\frac{5}{2},\frac{7}{2};2\alpha\right)$ is a generalized hypergeometric function, and $\mathrm{erfc}(\sqrt{2\alpha})$ is the complementary error function. So in the limit of $\bar{z} \to 0$,

$$(l\epsilon_x(\bar{z})) = 2A + (\frac{B}{2\alpha} - 2A)\bar{z}^2 + (\frac{C}{48\alpha^2} - \frac{B}{2\alpha} + A)\bar{z}^4 + (\frac{D}{2880\alpha^3} - \frac{C}{48\alpha^2} + \frac{B}{4\alpha} - \frac{A}{3})\bar{z}^6 \tag{B.28}$$

Since we know the expansion of $l\epsilon_x(\bar{z})$ at both $\bar{z} \to 0$ and $\bar{z} \to \infty$, we could apply the two-point padé approximation[28] to find a good parameterization of the $l\epsilon_x$.

The two-point padé approximation of $l\epsilon_x$ can be expressed as the quotient of two (m+1) by (m+1) determinants det$P(\bar{z})$ and det$Q(\bar{z})$ as:

$$(l\epsilon_x(\bar{z})) = \frac{\det P(\bar{z})}{\det Q(\bar{z})} + \frac{a_0}{2} \tag{B.29}$$

Here we choose $m = 6$, and we use an expansion up to $\bar{z}^6$ at $\bar{z} \to 0$ and the expansion at $\bar{z} \to \infty$ up to $\frac{1}{\bar{z}^5}$, so the two matrix has the following form.

$$Q(\bar{z}) = \begin{bmatrix} 1 & \bar{z} & \bar{z}^2 & \bar{z}^3 & \bar{z}^4 & \bar{z}^5 & \bar{z}^6 \\ a_6 & 0 & a_4 & 0 & a_2 & 0 & a_0 \\ 0 & a_4 & 0 & a_2 & 0 & a_0 & a_{-1} \\ a_4 & 0 & a_2 & 0 & a_0 & a_{-1} & a_{-2} \\ 0 & a_2 & 0 & a_0 & a_{-1} & a_{-2} & 0 \\ a_2 & 0 & a_0 & a_{-1} & a_{-2} & 0 & a_{-4} \\ 0 & a_0 & a_{-1} & a_{-2} & 0 & a_{-4} & 0 \end{bmatrix} \tag{B.30}$$

$$P(\bar{z}) = \begin{bmatrix} S_5 & \bar{z}S_4 & \bar{z}^2S_3 & \bar{z}^3S_2 & \bar{z}^4S_1 & \bar{z}^5S_0 & \frac{a_0}{2}\bar{z}^6 \\ a_6 & 0 & a_4 & 0 & a_2 & 0 & a_0 \\ 0 & a_4 & 0 & a_2 & 0 & a_0 & a_{-1} \\ a_4 & 0 & a_2 & 0 & a_0 & a_{-1} & a_{-2} \\ 0 & a_2 & 0 & a_0 & a_{-1} & a_{-2} & 0 \\ a_2 & 0 & a_0 & a_{-1} & a_{-2} & 0 & a_{-4} \\ 0 & a_0 & a_{-1} & a_{-2} & 0 & a_{-4} & 0 \end{bmatrix} \tag{B.31}$$

where a_6, a_4, ... a_{-4} are from the equations (B.26,B.28), and

$$S_k = \frac{a_0}{2} + a_1\bar{z} + ... + a_k\bar{z}^k \tag{B.32}$$

Note: we found when $\alpha \approx 0.001 \sim 0.01$, there is a sigularity showing up for $\bar{z} \approx 20 \sim 80$. This may have no effect for our final purpose of functional construction. we record it here for future possible problems. The problem may be solved by using an odd m padé approximation.

Overall, we have a parameterization of $l\epsilon_x$ based on density information, $l\epsilon_x(s,q)$, which can be converted to a function of auxilliary variables α and $\bar{z}$, $l\epsilon_x(\alpha(s,q),\bar{z}(s,q))$. The expression of $l\epsilon_x(\alpha,\bar{z})$ can be found in Eq.(B.29), and $\alpha(s,q)$ and $\bar{z}(s,q)$ can be found in Eq.(B.13,B.14). The α and $\bar{z}$ can also be derived from s and t using Eqs. (B.21,B.21). The will use s and t as basic ingredient for our functional in the following.

We need to get rid of the l for real application, hence we need the refinement factor F_x. For the HO with $\alpha \leq 1.0$, we have

$$(l\epsilon_x^{LDA}(\alpha,\bar{z})) = -\frac{3}{4\pi}(3\pi^{1/2}e^{-\bar{z}^2}\alpha)^{1/3} \tag{B.33}$$

So we our final form of refinement factor is:

$$F_x(s,t) = F_x(\alpha(s,t), \bar{z}(s,t)) = \frac{l\epsilon_x(\alpha, \bar{z})}{l\epsilon_x^{LDA}(\alpha, \bar{z})} \tag{B.34}$$

where $l\epsilon_x(\alpha, \bar{z})$ and $l\epsilon_x^{LDA}(\alpha, \bar{z})$ are respectively from Eq.(B.29) and Eq.(B.33).

For HO gas with $\alpha > 1.0$, the above parameterizations can not be applied directly. The main concern is that at $\bar{z} = 0$, Eq.(B.34) will not work for $\alpha > 1$. We know as α increases, the region around $\bar{z}$ will gradually approach the uniform electron gas (UEG) limit. For UEG, we have $t = 1$ and $s = 0$. According to Eq.(B.21) and (B.21), the mapped $\bar{z}$ and α are respectively 0 and $243\pi/125$. In such a case, we obtain a refinement factor $F_x = 1/1.01798$, which we should be 1. Thus to recover the proper description of the UEG situation, an extra term is multiplied to the original F_x, and the new refinement factor becomes:

$$F_x^{HO}(s,t) = F_x(\alpha(s,t), \bar{z}(s,t)) = (1 + \frac{0.03596}{1 + e^{(243\pi/125-\alpha)}})\frac{l\epsilon_x(\alpha, \bar{z})}{l\epsilon_x^{LDA}(\alpha, \bar{z})} \tag{B.35}$$

Now when we have a UEG situation, correct $F_x = 1$ is obtained, and as $\alpha < 1$, the original equation (B.34) is recovered.

Above parameterization works fine in the HO systems. However, in practical calculations, it occurs that ELF and s can be both small simultaneously, which leads to very large α. This situation can not find its counterpart in the HO model systems. Therefore to let the functional able to treat such situations, the α is reformulated to prevent too large α:

$$\alpha = \frac{\alpha}{1 + e^{(\alpha - \frac{243\pi}{125})}} + \frac{\frac{243\pi}{125}}{1 + e^{(\frac{243\pi}{125} - \alpha)}}; \tag{B.36}$$

This modification is applied to the α obtained through Eq. $B.21$.

When applying the above functionals on HO gas with $\alpha > 1$, over the edge regions, there is discrepancy between the results from current functional and the exact values for the ϵ_x. These regions can be well described by AM05, so we need an interpolation index to combine the AM05 and current functional. The interpolation index we choose is based on the ELF, which take the form of $f(ELF) = \frac{1}{1+e^{a(b-ELF)}}$. Empirically parameters $a = 15$ and $b = 0.65$ are obtained. So the final form for the refinement factor is:

$$F_x^{HAM} = \frac{F_x^{HO}}{1 + e^{15(0.65-ELF)}} + \frac{F_x^{AM05}}{1 + e^{15(ELF-0.65)}} \tag{B.37}$$

In the last the correlation energy functional need to be determined. We pick the similar form as the AM05, and the parameters are obtained by fitting to the Jellium surface exchange-correlation energy.

$$\epsilon_c^{HAM} = \epsilon_c^{LDA}\frac{1 + 0.0545s^2}{1 + 0.5196s^2} \tag{B.38}$$

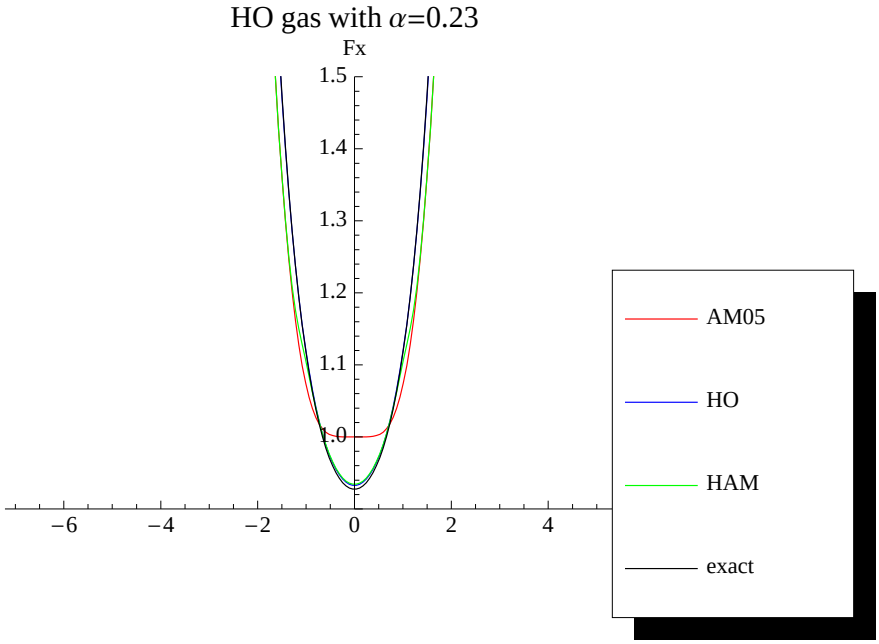

Figure B.1. The exchange energy for a strongly confined system. The AM05 exchange functional (red) gives a large error compared to the exact results (black). This error is mostly eliminated by the use of the HAM exchange functional (green). The HAM functional uses a parametrisation of the exact exchange which in this figure is shown in blue.

In Figure B.1 we see that the exchange part of the HAM functional reproduces the exact exchange energy in the high density parts of a strongly confined HO system reasonably well.

DISTRIBUTION:

1 Dr. John M. Wills
Los Alamos National Laboratory, T-1 MS B221 PO Box 1663
Los Alamos, NM 87545

1 Dr. Feng Hao
6620 Gessner Drive, Apt 3208
Houston, TX 77040

1 Dr. Rickard Armiento
929 Massachusetts Avenue, Apt 6G
Cambridge, MA 02139

1 Professor Mark Lusk
Dept. of Physics, Colorado School of Mines
Golden, CO 80401

1 Ms. Torey Semi
Dept. of Physics, Colorado School of Mines
Golden, CO 80401

1 Dr. Andrew C. Pineda
Dept. of Electrical and Computer Engineering, University of New Mexico
Albuquerque, NM 87131

1 Dr. Thomas A. Mehlhorn
2181 Jamieson Ave #3-2007
Alexandria, VA 22314-5756

1	MS 1189	Michael P. Desjarlais, 01640
1	MS 1189	Thomas R. Mattsson, 01641
1	MS 1191	John L. Porter, 01670
1	MS 1193	Briggs Atherton, 01672
1	MS 1318	Bruce A. Hendrickson, 01440
1	MS 1322	John A. Aidun, 01425
1	MS 1322	George Cragg, 01443
1	MS 1322	Rudolph J. Magyar, 01443
1	MS 1322	Peter A. Schultz, 01425
1	MS 1322	Ann E. Mattsson, 01443
1	MS 1323	John H. Carpenter, 01443
1	MS 1323	Erik O. Strack, 01443
1	MS 0899	RIM-Reports Management, 9532 (electronic copy)
1	MS 0359	D. Chavez, LDRD Office, 1911

Sandia National Laboratories